
NMR and μ SR in Highly Frustrated Magnets

Pietro Carretta¹ and Amit Keren²

1- Dipartimento di Fisica "A.Volta" - University of Pavia - Via Bassi, 6 - 27100 Pavia (Italy) carretta@fiscavolta.unipv.it

2- Technion-Israel Institute of Technology, Physics Department, Haifa 32000, Israel keren@physics.technion.ac.il

Hereafter we shall present a brief overview on some of the most significant achievements obtained by means of NMR and μ SR techniques in highly frustrated magnets. First the basic quantities measured by the two techniques will be presented and their connection to the microscopic static and dynamical spin susceptibility recalled. Then the main findings will be outlined, starting from the most simple frustrated units, the molecular nanomagnets, to artificially built frustrated systems as ^3He on graphite, to magnets with a macroscopically degenerate ground-state as the ones on a pyrochlore or kagomé lattices.

1 Some basic aspects of NMR and μ SR techniques

NMR and μ SR are very powerful techniques which allow to investigate the microscopic properties of spin systems through the study of the time evolution of the nuclear magnetization $\mathbf{M}(t)$ and of the muon spin polarization $\mathbf{P}(t)$, respectively [1, 2]. Each technique has its advantages and disadvantages. In NMR one knows the crystallographic position of the nuclei under investigation and, therefore NMR results can be more suitably compared to theories. On the other hand, NMR experiments cannot be performed in compounds where just low sensitivity nuclei are present or where the fast nuclear relaxations prevent the observation of an NMR signal. Still, polarized muons can be injected into the sample and used as a probe of the local microscopic properties of the system under investigation. Moreover, by means of μ SR it is possible to detect relaxation times shorter than $0.1 \mu\text{s}$, about two order of magnitudes shorter than the shortest relaxation time NMR can measure. Since the nuclear magnetization is the quantity detected in the NMR experiments, generally a magnetic field has to be applied to generate it. On the other hand, the muon beam is already polarized before entering the sample, so that the system under investigation can also be studied in zero field by means of μ SR. This aspect is particularly relevant if one wants to investigate the intrinsic properties of a certain system without perturbing it with a magnetic field. Nevertheless,

novel ground-states can be induced by the application of high magnetic fields (typically above 10 Tesla) where μ SR experiments cannot be performed while NMR experiment can. Hence, although both techniques appear to measure similar quantities (see next section), in view of the above considerations they are often complementary and their combination is a rather powerful method to investigate the local microscopic properties of frustrated magnets.

1.1 Line shift and line width

The time evolution of $\mathbf{M}(t)$ and $\mathbf{P}(t)$ is determined by the hyperfine interactions which can be summarized in the form

$$\mathcal{H} = \mathcal{H}_z + \mathcal{H}_{n-n} + \mathcal{H}_{n-e} + \mathcal{H}_{EFG} . \quad (1)$$

The effect of all the four terms on the hyperfine levels and on the NMR spectra for $I = 3/2$ are depicted in Fig. 1. We recall that the intensity of the whole spectrum is proportional to the nuclear magnetization. The first term

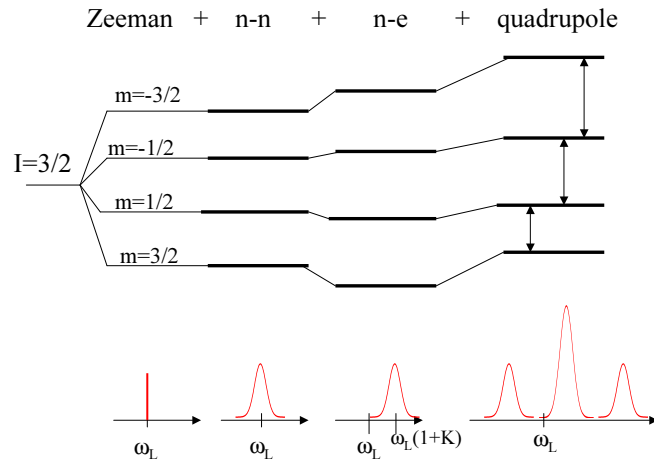


Fig. 1. Schematic illustration of the modifications in the hyperfine levels of $I = 3/2$ nuclei, due to the different terms of the nuclear hyperfine Hamiltonian. The corresponding modifications in the NMR spectra are reported at the bottom of the figure.

describes the Zeeman interaction with an external field, while \mathcal{H}_{n-n} is the dipole-dipole interaction among the nuclear spins or between the muon and the nuclear spins. This interaction yields a broadening of the NMR [1] and μ SR [2] spectra. In certain compounds, as the cuprates, the nuclear dipole-dipole interaction is mediated by the electron spins and from the dipolar broadening information on the static electron spin susceptibility $\chi'(\mathbf{q})$ is obtained [3]. The last term \mathcal{H}_{EFG} describes the interaction between the nuclear electric

quadrupole moment Q and the electric field gradient (EFG) generated by the charge distribution around the nucleus. This term is non-zero when the nuclear spin $I > 1/2$ and is, of course, absent in the muon interaction Hamiltonian. The quadrupole interaction is very sensitive to the modifications in the local configuration and allows to evidence distortions induced by the spin-lattice coupling [4] or the presence of a non-homogeneous charge distribution induced by charge ordering, for instance [5]. The third term is the most relevant one to probe frustrated magnetism, as it describes the hyperfine interaction with the electron spins \mathbf{S} . As most of the systems we shall be dealing with in the following are insulators, one can write

$$\mathcal{H}_{n-e} = -\gamma\hbar \sum_{i,k} \mathbf{I}_i \tilde{A}_{ik} \mathbf{S}_k \quad (2)$$

with \tilde{A}_{ik} the hyperfine coupling tensor, I and S are the nuclear/ μ^+ and electronic spin operator respectively, i and k are the nuclear/ μ^+ and electron spin indexes, respectively, while γ the nuclear (μ^+) gyromagnetic ratio. Then, the hyperfine field at the i -th nucleus/ μ^+ will be given by $\mathbf{h}_i = \sum_k \tilde{A}_{ik} \mathbf{S}_k$ and in the presence of a non-zero average polarization $\langle \mathbf{S} \rangle$ $\mathbf{h}_i = \sum_k \tilde{A}_{ik} \langle \mathbf{S}_k \rangle$. Thus, one can directly estimate $\langle \mathbf{S} \rangle$ from the precessional frequency $\omega = \gamma \sum_k \tilde{A}_k \langle \mathbf{S}_k \rangle$ of the nuclei or of the muons around the local field.

When an external field $\mathbf{H}_0 \parallel \hat{z}$ is applied the local magnetic field becomes

$$\mathbf{B} = \mathbf{H}_0 + \sum_k \tilde{A}_k \langle \mathbf{S}_k \rangle \quad (3)$$

and the resonance frequency will be shifted to

$$\omega = \omega_L(1 + K) \quad (4)$$

with $\omega_L = \gamma H_0$ the Larmor frequency and, for $H_0 \gg |\sum_k \tilde{A}_k \langle \mathbf{S}_k \rangle|$,

$$K = \frac{\left(\sum_k \tilde{A}_k \langle \mathbf{S}_k \rangle \right)_z}{H_0}. \quad (5)$$

In general K is a tensor and $\tilde{K} = \sum_k \tilde{A}_k \tilde{\chi}(\mathbf{q} = 0, \omega = 0)$. Hence, one notices that from the shift in the precessional frequency of the nuclei (or μ^+) one can derive the static uniform susceptibility associated only with those electron spins which are coupled to the nuclei under investigation see Fig.2.

If, for some reason, the distance between nuclei or muon and the electronic spins is random or there are missing spins in the sample, the hyperfine coupling \tilde{A} will be a random variable leading to a distribution of precessional frequencies and to an increase in the relaxation of the polarization/magnetization. For an external field applied perpendicular to the initial polarization of the muons one finds

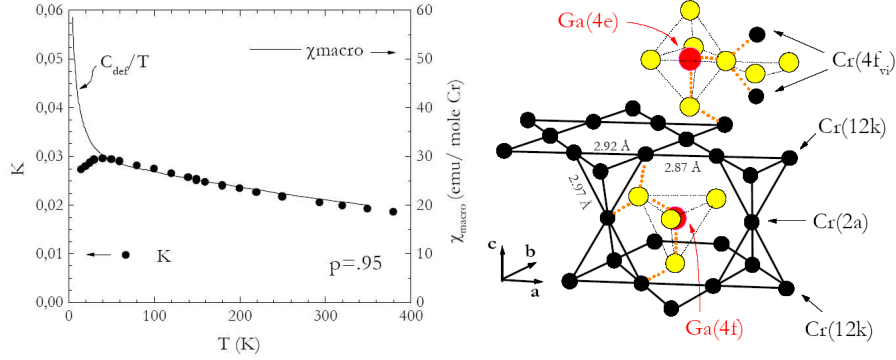


Fig. 2. Temperature dependence of $^{71}\text{Ga}(4f)$ NMR shift K in $\text{SrCr}_{9p}\text{Ga}_{12-9p}\text{O}_{19}$ ($p = 0.95$) compared to the macroscopic susceptibility derived with a magnetometer. Since $^{71}\text{Ga}(4f)$ nuclei are strongly coupled only to chromium ions within the kagomé bilayer one can single out just the intrinsic susceptibility of the latter, whereas the macroscopic susceptibility detects also the contribution from defects.[6]

$$P_{\perp}(t) = \exp\left(-\left[\frac{t}{T_2^*}\right]^2\right) \cos(\omega t). \quad (6)$$

$1/T_2^*$ could also represent the decay rate of the NMR signal after an RF pulse. Assuming a distribution of hyperfine fields in the \hat{z} direction one can write \tilde{A}_k as a sum of a mean value \bar{A}_k plus a fluctuating component δA_k . For the distribution

$$\rho(\delta A_k) = \frac{1}{\sqrt{2\pi}\sigma_k} \exp\left(-\frac{\delta A_k^2}{2\sigma_k^2}\right),$$

one finds that

$$\frac{1}{T_2^*} = \gamma \left(\sum_k \sigma_k^2\right)^{1/2} \chi H_0 \quad (7)$$

is the width of the spectrum which has an average shift

$$K = \frac{\omega - \gamma H_0}{\gamma H_0} = \chi \sum_k \bar{A}_k. \quad (8)$$

If σ_k and \bar{A} are temperature independent parameters we expect

$$1/T_2^* \propto K \quad (9)$$

where the temperature is an implicit parameter. It is noticed that this proportionality is correct regardless of the form of the relaxation (6). The breakdown of the validity of Eq. 9 would indicate a modification in the hyperfine couplings, which is typically expected when lattice distortions take place (see

Sec's. 2.2 and 2.5). On the other hand, in certain systems, although the hyperfine coupling is constant, the spin polarization can be site-dependent. Then, Eq.9 no longer holds and the line broadening and its shape reflects the distribution of the local spin polarization.[7]

1.2 Nuclear and muon spin lattice relaxation rate $1/T_1$

The transitions among the hyperfine levels, driven by the time dependent part of the hyperfine Hamiltonian (not shown in Eq. 1), modify the nuclear spin population on each level, namely the longitudinal component of nuclear magnetization. Thus, in a frustrated magnet from the time evolution of the nuclear magnetization it is possible to derive information on the spin dynamics, which drives the fluctuations of the hyperfine field. The recovery of the longitudinal component of the nuclear magnetization, after the nuclear spin ensemble has been brought out of equilibrium with an *ad hoc* RF pulse sequence, is described by a characteristic decay rate $1/T_1$. In case of relaxation mechanisms driven by fluctuations of the hyperfine field $\mathbf{h}(t)$, by resorting to time-dependent perturbation theory (h is considered small with respect to H_0) and assuming that the frequency of the field fluctuations $\omega = 2\pi\nu \gg 1/T_1$, one can write

$$\frac{1}{T_1} = \frac{\gamma^2}{2} \int_{-\infty}^{+\infty} e^{i\omega_L t} \langle h_+(t)h_-(0) \rangle dt . \quad (10)$$

This fundamental expression shows that $1/T_1$ is driven by the transverse components of the fluctuating field at the nucleus, owing to magnetic-dipole selection rules, and that $1/T_1$ is proportional to the Fourier transform of the correlation function at the resonance frequency, in order to allow for energy conservation. In other terms $1/T_1$ probes the spectral density at the resonance frequency ω_L which is typically in the MHz range, orders of magnitude below the spectral range accessed by inelastic neutron scattering experiments. It should be noticed that this does not mean that from $1/T_1$ one cannot estimate relevant energy scales much larger than $\hbar\omega_L$. In fact, when sum rules apply, as it is often the case in spin systems, the amplitude of the low-frequency spectral density is determined by the characteristic frequency of the fluctuations $\omega \gg \omega_L$.

In general, when collective spin excitations are present one can write

$$\mathbf{h}(t) = \frac{1}{\sqrt{N}} \sum_{\mathbf{q}} \sum_k e^{i\mathbf{q}\mathbf{r}_k} \tilde{A}_k \mathbf{S}(\mathbf{q}, t) \quad (11)$$

and by substituting the transverse components of $\mathbf{h}(t)$ in Eq. 10 expression one finds that

$$\frac{1}{T_1} = \frac{\gamma^2}{2} \frac{1}{N} \sum_{\mathbf{q}, \alpha=x,y,z} \left(|A_{\mathbf{q}}|^2 S_{\alpha\alpha}(\mathbf{q}, \omega_L) \right)_{\perp} . \quad (12)$$

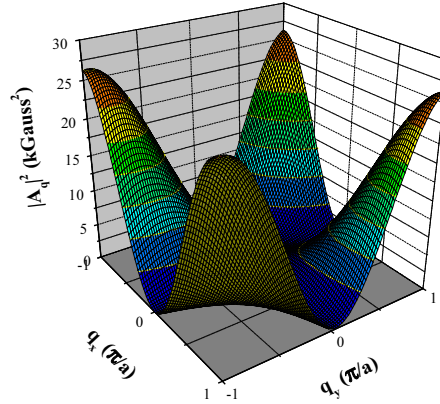


Fig. 3. ^{29}Si form factor in the first Brillouin zone of the two-dimensional frustrated antiferromagnet $\text{Li}_2\text{VOSiO}_4$. It is evident that excitations at wave-vectors $(\pm\pi/a, 0)$ or $(0, \pm\pi/a)$ are filtered out, namely that ^{29}Si $1/T_1$ is not sensitive to these modes.

One notices that, being the nuclei local probes, $1/T_1$ is related to the integral over the Brillouin zone of the component of the dynamical structure factor $S_{\alpha\alpha}(\mathbf{q}, \omega_L)$ at the Larmor frequency. In Eq. 12 $|A_{\mathbf{q}}|^2$ is the form factor which gives the hyperfine coupling of the nuclei with the spin excitations at wave-vector \mathbf{q} (see Fig. 3). The term \perp indicates that one has to consider the products $|A_{\mathbf{q}}|^2 S_{\alpha\alpha}(\mathbf{q}, \omega_0)$ associated with the perpendicular components of the hyperfine field at the nucleus. From the fluctuation-dissipation theorem, by recalling that usually $k_B T \gg \hbar\omega_L$ one can also write

$$\frac{1}{T_1} = \frac{\gamma^2 k_B T}{2 \hbar} \frac{1}{N} \sum_{\mathbf{q}, \alpha=x,y,z} \left(|A_{\mathbf{q}}|^2 \frac{\chi''_{\alpha\alpha}(\mathbf{q}, \omega_L)}{\omega_L} \right)_{\perp} \quad (13)$$

This rather general expression shows how the nuclear or muon spin-lattice relaxation is related to the spectrum of the excitations characteristic of each frustrated magnet.

The above equations apply also to μSR spin-lattice relaxation rate when a large magnetic field is applied. On the other hand, when μSR operates in zero field, standard perturbation methods to analyze the data, such as Eq. 10, are no longer valid. This is because the transverse direction is not defined and the internal field is not small compared to H . Accordingly, different methods are required to account for the muon relaxation function in zero and small external fields. Moreover, usually one does not know the muon stopping site, and therefore the discussion is done using the field at the muon site B rather than the hyperfine coupling A . The treatment of the muon T_1 in zero or small fields is done in two steps. The first step is the static case where $T_1 = \infty$. In the second step, the dynamic fluctuations are added and T_1 becomes finite.

1.3 μ SR: the static case

The fully polarized muon, after entering the sample, comes to rest in a magnetic environment. Since the mechanism which stops the muon is much stronger than any magnetic interaction, the muon maintains its polarization while losing its kinetic energy. Once the muon reaches its site, the muon spin starts to evolve in the local field \mathbf{B} . The muon polarization P_z along the $\hat{\mathbf{z}}$ direction is given by the double projection expression

$$P_z(\mathbf{B}, t) = \cos^2 \theta + \sin^2 \theta \cos(\gamma_\mu |\mathbf{B}| t) \quad (14)$$

where θ is the angle between the initial muon spin and the local field direction (see Fig. 4). This angle is related to the field values by

$$\cos^2 \theta = \frac{B_z^2}{\mathbf{B}^2}, \quad \sin^2 \theta = \frac{B_x^2 + B_y^2}{\mathbf{B}^2}.$$

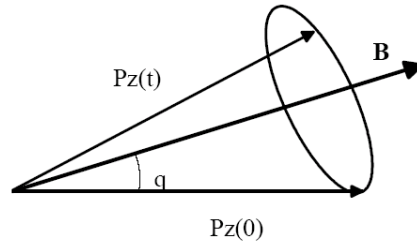


Fig. 4. Muon spin polarization rotating around a magnetic field in an arbitrary direction.

In a real sample, however, there will be a distribution of internal fields and the averaged polarization is

$$\bar{P}_z(t) = \int \rho(\mathbf{B}) \left[\frac{B_z^2}{\mathbf{B}^2} + \frac{B_x^2 + B_y^2}{\mathbf{B}^2} \cos(\gamma_\mu |\mathbf{B}| t) \right] d^3 \mathbf{B} \quad (15)$$

where $\bar{P}_z(t)$ is the sample averaged polarization, and $\rho(\mathbf{B})$ is the field distribution which is normalized according to $\int \rho(\mathbf{B}) d^3 \mathbf{B} = 1$. If the distribution of internal fields is only a function of $|\mathbf{B}|$ then we can write

$$\bar{P}_z(t) = \int \rho(|\mathbf{B}|) [\cos^2 \theta + \sin^2 \theta \cos(\gamma_\mu |\mathbf{B}| t)] B^2 dB d\Omega.$$

It is convenient to define $\rho'(|\mathbf{B}|) = 4\pi\rho(|\mathbf{B}|)$, so that $\int \rho'(|\mathbf{B}|) B^2 dB = 1$ and the angular dependence can be integrated out giving

$$\overline{P}_z(t) = \frac{1}{3} + \frac{2}{3} \int \rho'(|\mathbf{B}|) \cos(\gamma_\mu |\mathbf{B}| t) B^2 dB.$$

If, for example, the system has long range order the field at the muon site is centered around a specific value ω_0/γ_μ so that

$$\rho'(|\mathbf{B}|) = \frac{\gamma_\mu}{\sqrt{2\pi}\Delta B^2} \exp\left[-\gamma_\mu^2 \left(|\mathbf{B}| - \frac{\omega_0}{\gamma_\mu^2}\right)^2 / 2\Delta^2\right],$$

then

$$\overline{P}_z(\omega_0, \Delta, t) = \frac{1}{3} + \frac{2}{3} \exp\left(-\frac{\Delta^2 t^2}{2}\right) \cos(\omega_0 t)$$

and oscillations will be observed in the data. At long time the polarization will relax to 1/3 since effectively 1/3 of the muons experience a field parallel to their initial spin direction and do not relax.

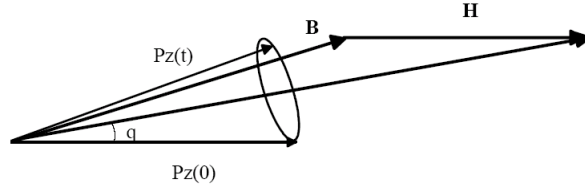


Fig. 5. Muon spin polarization rotating around the vector sum of an external magnetic field in the initial muon polarization direction, and an arbitrary internal field.

When a longitudinal field H is applied in the direction of the initial muon spin as in Fig. 5, the situation becomes more complicated, and there is no closed form expression. However, some simplifications could be made to reduce the dimension of the integrals for the purpose of numerical calculations. For example, if the local field is completely random with a Gaussian distribution then

$$\rho(\mathbf{B}) = \frac{\gamma_\mu^3}{(2\pi)^{3/2}\Delta^3} \exp\left(-\frac{\gamma_\mu^2[\mathbf{B}-H_0\hat{\mathbf{z}}]^2}{2\Delta^2}\right). \quad (16)$$

In this case Eq. 15 could be simplified to [8]

$$\begin{aligned} \overline{P}_z(\omega_L, \Delta, t) = 1 - \frac{2\Delta^2}{(\omega_L)^2} \left[1 - \exp\left(-\frac{1}{2}\Delta^2 t^2\right) \cos(\omega_L t) \right] + \\ \frac{2\Delta^4}{(\omega_L)^3} \int_0^t \exp\left(-\frac{1}{2}\Delta^2 \tau^2\right) \sin(\omega_L \tau) d\tau \end{aligned} \quad (17)$$

This is known as the static-Gaussian-longitudinal-field Kubo-Toyabe (KT) function. Figure 6 shows $\overline{P}_z(\omega_L, \Delta, t)$ for a variety of ω_L . Interestingly, despite the fact that the external field is in the muon spin direction, wiggles are seen

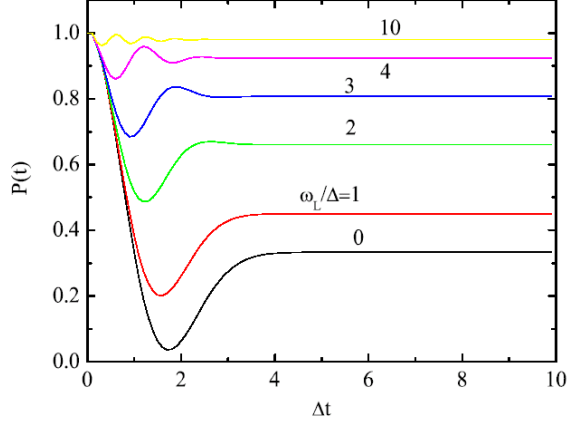


Fig. 6. Muon polarization function in a Gaussian internal field distribution and external field pointing in the initial muon spin direction. Different values of the external field H are shown.

in the polarization, and their frequency is given by ω_L . When $\omega_L \gg \Delta$, the muon does not relax any more because the field at the muon site is nearly parallel to the initial muon spin direction. In this situation we say that the external field decoupled the muon spin from the internal field. Finally, in the zero field case ($H_L = 0$) Eq. 17 reduces to [8]

$$\bar{P}_z(0, \Delta, t) = \frac{1}{3} + \frac{2}{3}(1 - \Delta^2 t^2) \exp(-\frac{1}{2}\Delta^2 t^2). \quad (18)$$

This polarization function is known as the static-Gaussian-zero-field KT. At early time it has a Gaussian-like behavior. It reaches a minimum on a time scale set by Δ after which it recovers and saturates again to $1/3$.

1.4 μ SR: the dynamic case

If we now add dynamics numerical methods must be applied. If the dynamic part of the local field at the muon site $\delta\mathbf{B}$ fluctuates in time and magnitude so that

$$\langle \delta\mathbf{B}(t)\delta\mathbf{B}(0) \rangle = \frac{3\Delta^2}{\gamma_\mu^2} \exp(-2\nu t), \quad (19)$$

where ν is a fluctuation rate, and under the strong collision approximation, the muon polarization will obey the Volterra equation of the second kind [13]. The polarization $\bar{P}_z(\nu, \omega_L, \Delta, t)$, which now also depends on the fluctuation rate ν , obeys

$$\begin{aligned} \bar{P}_z(\nu, \omega_L, \Delta, t) = & e^{-\nu t} \bar{P}_z(0, \omega_L, \Delta, t) + \\ & \nu \int_0^t dt' \bar{P}_z(\nu, \omega_L, \Delta, t-t') e^{-\nu t'} \bar{P}_z(0, \omega_L, \Delta, t') \end{aligned} \quad (20)$$

where $\overline{P}_z(0, \omega_L, \Delta, t)$ is the static relaxation function, namely, the polarization if the local field was frozen in time. The factor $e^{-\nu t}$ is the probability to have no field changes up to time t . The factor $e^{-\nu t'} \nu dt'$ is the probability density to experience a field change only between t' and $t' + dt'$. The first term on the r.h.s is the polarization at time t due to muon that did not experienced any field changes. The second term on the r.h.s is the contribution from those muon that experience their first field change at time t' . The factor $e^{-\nu t'} \overline{P}_z(0, H, \Delta, t') \nu dt'$ is the amplitudes for the polarization function that evolves from time t' to t , which can involve more field changes recursively. This equation can be solved numerically [10].

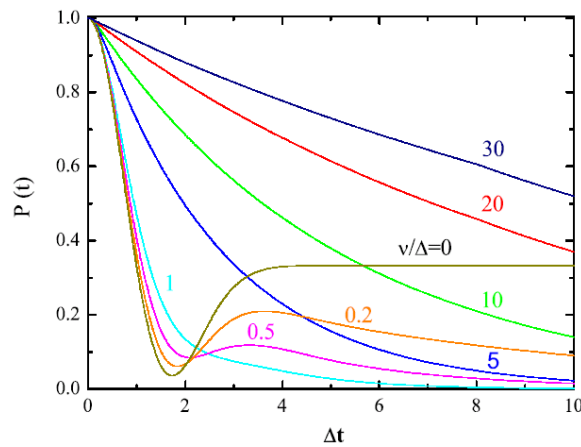


Fig. 7. Expected muon relaxation in a dynamic field with Gaussian instantaneous distribution and no external field. Different values of fluctuation rates are shown.

There are three ways of using Eq. 20 to obtain dynamic information. The first is in simple cases where $\overline{P}_z(0, \omega_L, \Delta, t)$ is known analytically as was done by Brewer *et al.* [11] for F- μ -F bond. The second is when $\overline{P}_z(0, \omega_L, \Delta, t)$ must be obtained numerically as in the cases of Gaussian [8] or Lorentzian [12] field distribution with external longitudinal field. The third way is to measure $\overline{P}_z(0, \omega_L, \Delta, t)$ by cooling the system to low enough temperatures that dynamic fluctuations are no longer present, and to use the measured $\overline{P}_z(0, \omega_L, \Delta, t)$ as an input to the Volterra equation [13].

Taking the polarizations generated by static field distribution given by Eq. 17 with $\omega_L = 0$, and using it as an input in the Volterra equation, gives the dynamic polarizations shown in Fig. 7. We see from this figure that when dynamic fluctuations are present the 1/3 recovery is lost. As the fluctuation rate ν increases, the Gaussian-like relaxation at $t \rightarrow 0$ is also lost, and when $\nu > \Delta$ the relaxation becomes exponential.

Finally, in Fig. 8 we present the most complicated relaxation function combining Gaussian field distribution, fluctuations, and longitudinal field. This is known as the dynamic-Gaussian-longitudinal-field-KT relaxation function. We have chosen a special value of the parameters $\Delta = 11.8$ MHz and $\nu = 12.2$ MHz for reasons that will become clear in Sec. 2.5, and show how the polarization is modified as H varies.

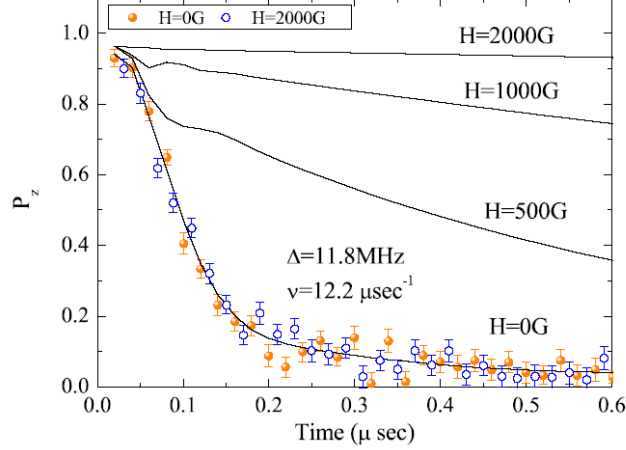


Fig. 8. Solid lines: Expected muon relaxation in a combination of internal field fluctuations with Gaussian instantaneous distribution, and longitudinal external field H . Symbols: Relaxation data from $\text{SrCr}_{9p}\text{Ga}_{12-9p}\text{O}_{19}$ from Ref. [42] in two different values of H . The disagreement between data and model indicates unusual behavior and is discussed in Sec. 2.5

It is interesting to mention that for the case $\nu \geq \Delta$ there is an approximate expression for the dynamic-Gaussian-longitudinal-field-KT relaxation function [14] given by

$$\overline{P}_z(t) = \exp(-\Gamma(t)t) \quad (21)$$

where

$$\Gamma(t)t = \frac{2\Delta^2 \{ [\omega_L^2 + \nu^2]\nu t + [\omega_L^2 - \nu^2][1 - e^{-\nu t} \cos(\omega_L t)] - 2\nu\omega_L e^{-\nu t} \sin(\omega_L t) \}}{(\omega_L^2 + \nu^2)^2}$$

In the long time limit ($\nu t \gg 1$) one finds that $\lim_{t \rightarrow \infty} \overline{P}_z(t) = P_0 \exp(-t/T_1)$ leading to the standard expression for T_1

$$\frac{1}{T_1} = \frac{2\Delta^2\nu}{(\omega_L^2 + \nu^2)}. \quad (22)$$

This expression demonstrates that when the external field is small, namely, $\omega_L \ll \nu$, T_1 will show no field dependence. But when the field is large $\omega_L \gg \nu$, T_1 will increase with increasing field. Therefore, field dependent measurements can be used to provide information on ν , and distinguish between static and dynamic cases.

Equation 22 could be related to Eq. 13 given for NMR $1/T_1$. In systems characterized by a spin-spin correlation function decaying in time as $\exp(-\nu t)$, neglecting the q -dependence, one can write for the spin susceptibility

$$\chi''_{\alpha\alpha}(0, \omega) = \frac{(g\mu_B)^2}{\hbar V} \frac{\hbar\omega}{k_B T} N \langle S_\alpha^2 \rangle \frac{\nu}{\nu^2 + \omega^2},$$

so that Δ^2 in Eq. 22 can be related to the amplitude of the spin fluctuations

$$\Delta^2 = \frac{\gamma^2}{12} S(S+1) \sum_{\mathbf{q}} (|A_{\mathbf{q}}|^2)_{\perp}.$$

When the applied field is small or the fluctuations are fast Eq. 22 reduces to

$$\frac{1}{T_1} = \frac{2\Delta^2}{\nu}. \quad (23)$$

Typical values are $T_1 \sim 0.1 \mu\text{sec}$, $\Delta \sim 10 \text{ MHz}$, and $\nu \sim 10 \mu\text{sec}^{-1}$.

2 From zero to three-dimensional frustrated magnets

2.1 Molecular Magnets

In recent years major attention has been addressed to the study of molecular crystals containing molecules formed by paramagnetic ions with significant intramolecular exchange couplings and negligible intermolecular couplings, so that each one of them can be considered as an independent nanomagnet [15].

In some nanomagnets V^{4+} $S = 1/2$ ions form a triangular lattice. This is the case, for instance, of V_{15} , where at low temperature (T) 12 V^{4+} spins are coupled in singlets and the remaining 3 ions form a triangle. From the study of ^{51}V NMR shift below 100 mK Furukawa et al.[16] have preliminarily estimated the hyperfine coupling and then estimated the expectation values for V^{4+} magnetic moments in zero-field. The resonance frequency of the i -th nucleus is given by $\omega_i = \gamma(\mathbf{H}_0 + \tilde{A} \cdot \mathbf{S}_i)$, where the internal fields $\tilde{A} \cdot \mathbf{S}_i$ have a different orientation and magnitude, depending on $\langle \mathbf{S}_i \rangle$. In order to derive $\langle \mathbf{S}_i \rangle$ the authors have studied the magnetic field dependence of ω_i , as shown in Fig. 9. The expectation values were found to be consistent with a doubly degenerate ground-state of the form

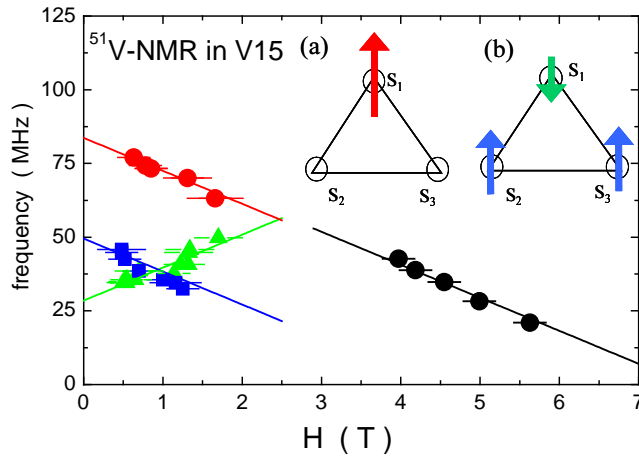


Fig. 9. Magnetic field dependence of the resonance frequency for different ^{51}V sites in V_{15} , used to derive the spin polarization of each V^{4+} [16]. In the inset the schematic view of the twofold degenerate ground-state is shown.

$$\begin{aligned} \psi_a &= \frac{1}{\sqrt{2}}(|\downarrow\downarrow\uparrow\rangle - |\downarrow\uparrow\downarrow\rangle) \\ \psi_a &= \frac{1}{\sqrt{6}}(|\uparrow\downarrow\downarrow\rangle - |\downarrow\uparrow\downarrow\rangle - |\downarrow\downarrow\uparrow\rangle) \end{aligned} \quad (24)$$

where \uparrow or \downarrow represents the orientation of each one of the three spins. μ SR longitudinal relaxation rate measurements in the same compound [17] evidenced a nearly T-independent relaxation rate at low temperature, which is possibly associated with the transitions among these two degenerate ground-states. If one considers that the frequency of the spin fluctuations $\omega \gg \omega_L$, one can derive the characteristic tunneling rate between the two degenerate states. We point out that a nearly T-independent relaxation is observed also in frustrated magnets with a macroscopically degenerate ground-state (see Sect. 2.6).

2.2 Antiferromagnets on a square-lattice with competing interactions: the $J_1 - J_2$ model

V^{4+} ions can also form other magnetic structures characterized by a strong frustration of the magnetic moments. In fact, certain vanadates can be considered as prototypes of frustrated magnets on a square lattice where frustration arises from the competition between nearest neighbour (J_1) and next-nearest neighbour (J_2) exchange couplings. The first NMR studies have been carried out in $\text{Li}_2\text{VOSiO}_4$. ^7Li NMR spectra were observed to split in three different

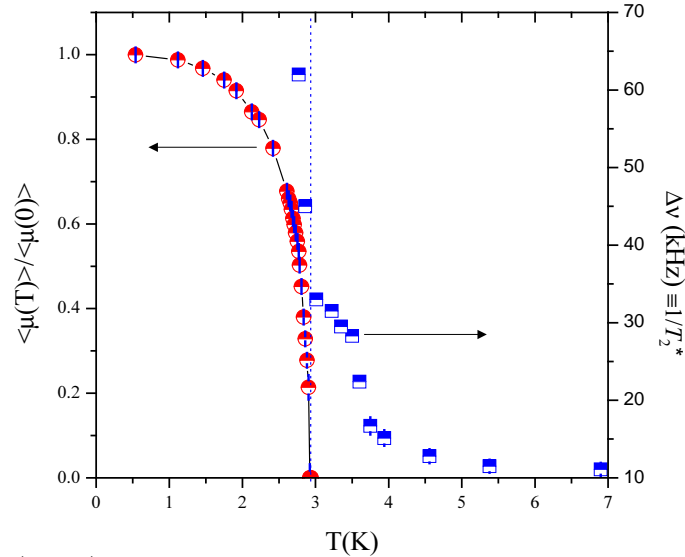


Fig. 10. (circles) Temperature dependence of the order parameter in the collinear phase of $\text{Li}_2\text{VOSiO}_4$, derived from zero-field μSR . (squares) Temperature dependence of ${}^7\text{Li}$ NMR linewidth for $\mathbf{H} \parallel ab$ in $\text{Li}_2\text{VOSiO}_4$. It is noticed that a broadening starts well above the transition temperature (vertical dotted line) and is possibly due to a frustration driven lattice distortion.

lines for $T < T_c \simeq 2.9$ K [18, 19], one unshifted and the other two symmetrically shifted with respect to the central one. This splitting of the NMR line was the first evidence that this compound is characterized by a magnetic collinear ground-state, as confirmed few years later by neutron scattering experiments [20]. A careful study of the order parameter has been carried out by means of zero-field μSR measurements (Fig. 10), where the μ^+ polarization is characterized by oscillations at a frequency directly proportional to V^{4+} magnetic moment [21] (Sect. 1). The continuous increase of the order parameter for $T \rightarrow T_c$ was found to be described by a critical exponent close to the one expected for 2D XY universality class. Above T_c , when no internal field is present, the NMR shift K is expected to be proportional to the static uniform spin susceptibility χ_s (see Eq. 5), with a slope given by the hyperfine coupling. Remarkably, for $T_c < T < J_1 + J_2$ a change in the slope of ${}^7\text{Li}$ K vs χ_s is noticed [22], suggesting a modification in the average hyperfine coupling (see Sect. I). Moreover, the broadening of ${}^7\text{Li}$ NMR linewidth in the same temperature range can be explained only if the distribution of the hyperfine couplings is also increasing in the same temperature range. We remark that in this temperature range the average shift decreases on cooling below 5 K while the linewidth increases, namely the breakdown of Eq. 9 is noticed. A similar scenario is observed for ${}^{95}\text{Mo}$ NMR in MoVO_5 [23]. These modifications in

the hyperfine coupling have been associated with a lattice distortion driven by the spin-lattice coupling, which releases the degeneracy of the magnetic ground-state.

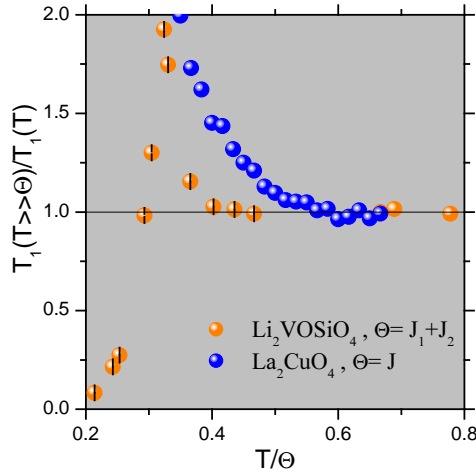


Fig. 11. Comparison of the temperature dependence of ${}^7\text{Li}$ $1/T_1$ in $\text{Li}_2\text{VOSiO}_4$ with ${}^{63}\text{Cu}$ $1/T_1$ in La_2CuO_4 , where frustration is negligible. The temperature is normalized to Curie-Weiss temperature Θ , while $1/T_1$ is normalized to its value at $T \gg \Theta$.

The T -dependence of the in-plane correlation length ξ of $\text{Li}_2\text{VOSiO}_4$ has been estimated from ${}^7\text{Li}$ $1/T_1$ [24]. In fact, by resorting to scaling arguments one can rewrite the dynamical structure factor in Eq. 12 in terms of powers of ξ . One finds

$$\frac{1}{T_1} \sim \xi^z \sim \exp(2\pi z \rho_s/T). \quad (25)$$

with ρ_s the spin stiffness and z the dynamical scaling exponent which is estimated around $z = 1$ on the basis of some physical considerations [24]. It turns out that for a two-dimensional antiferromagnet on a square-lattice frustration yields a less pronounced increase of ξ on cooling, namely to a decrease in the spin stiffness.

The decay of the longitudinal muon polarization in $\text{Li}_2\text{VOSiO}_4$ and $\text{Li}_2\text{VOGeO}_4$ was observed to be well described by Eq. 18 and evidenced a dynamics at frequencies well below the Heisenberg exchange frequency [24]. This dynamic has been ascribed to the fluctuations within the two-fold degenerate ground-state over a barrier [25]

$$E(T) = \left(\frac{J_1^2 S^2}{2J_2} \right) \left[0.26 \left(\frac{1}{S} \right) + 0.318 \left(\frac{T}{J_2 S^2} \right) \right] \xi^2(T) .$$

2.3 Magnetic frustration on a triangular lattice

The simplest two-dimensional lattice frustrated by the geometry of the interactions is the triangular one. Several systems on a triangular lattice have been investigated in the last decade, either insulating [26] or metallic ones [27]. Some of these compounds display a rather interesting phase diagram as a function of the magnetic field intensity, as will be shown in a subsequent chapter of this book by M. Takigawa and F. Mila. Also in κ -(ET)₂Cu₂(CN)₃ molecular crystals, which are insulators at ambient pressure, the spins are arranged on a triangular lattice. Recently, it has been observed (Fig.12) that ¹H $1/T_1$ abruptly decreases at low temperature [28]. This decrease can be associated with the onset of a gap Δ between a collective singlet and triplet states, which yields $1/T_1 \propto \exp(-\Delta/T)$ for $T \ll \Delta$, and can be considered the first evidence for a spin-liquid phase in a triangular antiferromagnet. This could be possibly the experimental evidence of the long sought RVB state predicted by Anderson long ago [29]. Interestingly enough the application of hydrostatic pressure was observed to drive this system into a superconducting ground-state which can still be justified in terms of an RVB description.

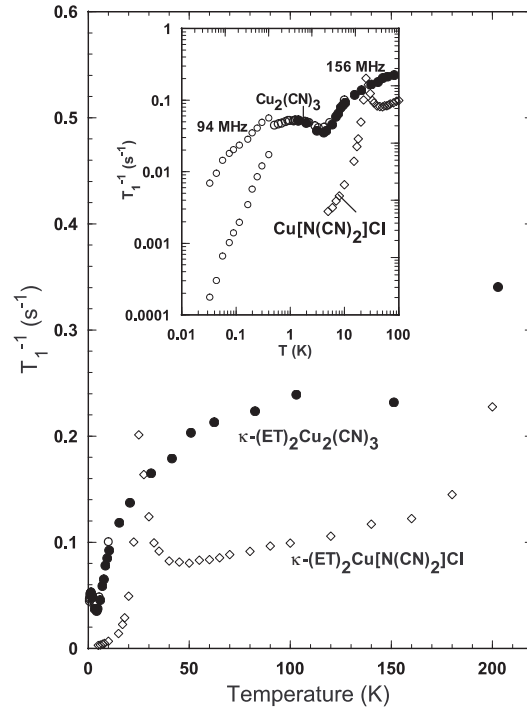


Fig. 12. ¹H nuclear spin-lattice relaxation rate $1/T_1$ for a single crystal (open circles) and a polycrystalline sample (closed circles) of κ -(ET)₂Cu₂(CN)₃ and a single crystal of κ -(ET)₂Cu[N(CN)₂]Cl (open diamonds) [28]. The Inset shows the low temperature part of the data in logarithmic scales.

Another spin system on a triangular lattice which has attracted much attention in recent years is Na_xCoO_2 , where a rich phase diagram develops upon Na doping [30]. An accurate study of the ^{23}Na and ^{59}Co NMR spectra in oriented powders evidenced a charge order for $x \simeq 0.7$ [5]. The signature of the charge order is the presence of three distinct Na sites characterized by different quadrupole couplings and magnetic shifts, which imply a well defined order of the Na^+ ions and of the Co charges in the CoO_2 planes. On the other hand, for $x = 0.5$ the study of the temperature dependence of ^{59}Co NMR spectra reveals that the electric field gradient at the Co site does not change at the metal-insulator transition, indicating the absence of any charge ordering [31]. These NMR measurements have allowed to clarify the nature of the ground-state of this system in the doping range $0.5 \leq x \leq 0.75$ [32]. When full Na doping is achieved the system eventually becomes non-magnetic and the NMR shift vanishes [33]. Remarkably for $x = 0$ the isostructural compound CoO_2 is found to be metallic, with a crossover from a strongly correlated metal to a Fermi-liquid behaviour at low temperature [34]. In fact, around 4 K the temperature dependence of $1/T_1T$ starts to flatten, as expected in a Fermi-liquid [1].

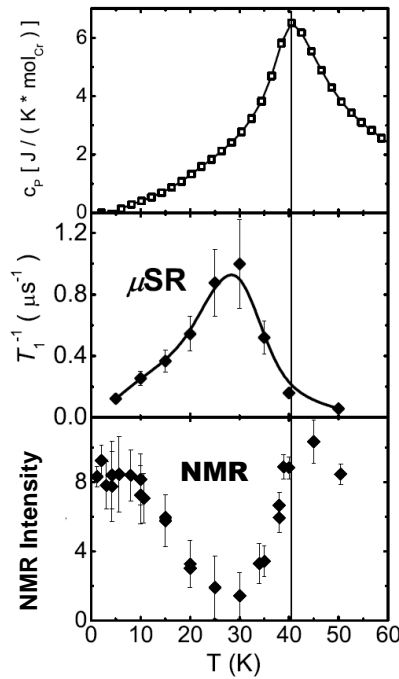


Fig. 13. From the top: specific heat, muon spin-lattice relaxation rate and ^{23}Na NMR signal intensity in NaCrO_2 vs. temperature. It is noticed that the peak in the specific heat and $1/T_1$ occur at different temperatures. The loss of ^{23}Na signal is possibly associated with an increase of the NMR relaxation rates.

Recently, it has been pointed out that NaCrO_2 is an excellent realization of a $S = 3/2$ triangular Heisenberg antiferromagnet. Remarkably, in this compound while specific heat and magnetization measurements indicate the onset of a transition around $T_c \simeq 40$ K, both muon spin rotation and NMR reveal a fluctuating crossover regime extending well below T_c , with a peak in $1/T_1$ around 25 K [35] (see Fig.13). This apparent discrepancy might indicate the presence of vortex-antivortex excitations decoupling around 25 K.

Magnetic frustration can be associated not only with the geometry of the electron spin arrangement but also with the one of indistinguishable nuclear spins, as it is the case for ^3He . The triangular lattice topology can be achieved by evaporating a single layer of ^3He on a graphite substrate. Then one can conveniently use the intensity of the NMR signal, which is proportional to the nuclear magnetization, to track the T dependence of the nuclear spin susceptibility [36]. ^3He NMR measurements have been carried out down to tens of μK , more than an order of magnitude below the exchange coupling. The low temperature increase in the nuclear spin susceptibility evidenced the relevance of higher order multiple spin exchange interactions which, together with the triangular geometry of the nuclear spins, makes the system strongly frustrated and possibly characterized by a gapless spin-liquid ground-state [37, 36].

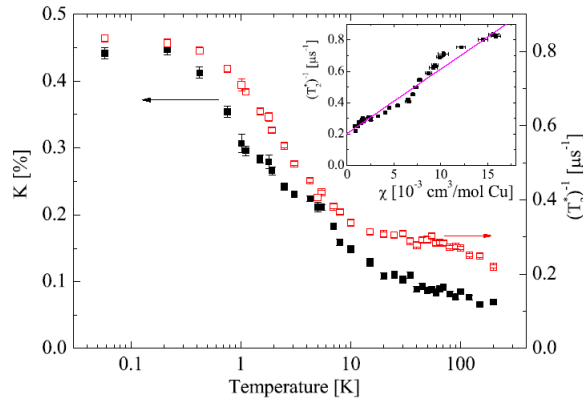


Fig. 14. The muon shift K and transverse relaxation time $1/T_2^*$, versus temperature. Inset, a plot of $1/T_2^*$ versus the system's susceptibility.

2.4 μSR and NMR in the spin-1/2 kagomé lattice $\text{ZnCu}_3(\text{OH})_6\text{Cl}_2$

A very interesting model compound for the study of magnetism on the kagomé lattice is the herbertsmithite $\text{ZnCu}_3(\text{OH})_6\text{Cl}_2$. The moments in this material originate from Cu^{2+} which has a spin 1/2. Therefore, it is ideal for the investigation of quantum ground states. Unfortunately, different probes such as

muon [38], O, [39] Cu, and Cl [40] nuclear magnetic resonance suggest different behavior of the shift below ~ 50 K and the origin of these variations are not clear yet. Here we present only the μ SR results. First we examine the muon shift and T_2^* in $\text{ZnCu}_3(\text{OH})_6\text{Cl}_2$ independently (Fig. 14), and also one as a function of the other (inset of Fig. 14). The shift, and hence the susceptibility, increase continuously upon cooling and saturate below 200 mK. This indicates that the spin-1/2 kagomé does not freeze or form singlets. The ground state is paramagnetic. In addition, the K and $1/T_2^*$ follow each other as the temperature is lowered, as shown in the inset, as expected from Eq. 9. Although K is not exactly a linear function of $1/T_2^*$ there is no reason to suspect a modification in the hyperfine coupling upon cooling, namely that lattice deformation is present in this case.

Second we examine whether the ground state is separated by a gap from the excited ones. If such a gap exists it will take a finite temperature to generate excitations and achieve a non zero $\chi''_{\alpha\alpha}(\mathbf{q}, \omega_0)$. Therefore, according to Eq. 13, $1/(T_1T)$ should extrapolate to zero. This has not been observed experimentally [41, 40, 39]. The ^{37}Cl $1/T_1$ depicted in Fig. 15 is proportional to T meaning that $\chi''_{\alpha\alpha}(\mathbf{q}, \omega_0)$ is finite in the $T \rightarrow 0$ limit. Therefore, there is no evidence of a gap and the kagomé lattice seems to be an exotic magnet with no broken continuous symmetry but gapless excitations.

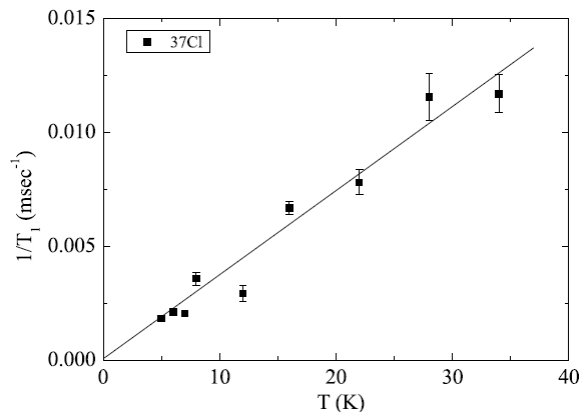


Fig. 15. ^{37}Cl $1/T_1$ in the herbertsmithite $\text{ZnCu}_3(\text{OH})_6\text{Cl}_2$ at low temperature.

2.5 The problem of the μ^+ relaxation in some kagomé lattices

At the very beginning of the research in the field of frustrated magnets it was noticed that the muon relaxation function is unusual [42]. The symbols in Fig. 8 show the polarization at a temperature of 100 mK in the kagomé system $\text{SrCr}_{9p}\text{Ga}_{12-9p}\text{O}_{19}$ (SCGO) in zero field and a longitudinal field of 2 kG [42].

First, no oscillations are found, so the internal field is random with either static or dynamic nature. Second, the relaxation at early time is Gaussian, with a time scale of $0.1 \mu\text{sec}$, so Δ must be on the order of 10 MHz. Third, there is no recovery so there must be some dynamic as in Fig. 7. But it must be that $\nu \sim \Delta$. Had ν been larger than Δ , the initial relaxation would have been Lorentzian (See Eq. 21 to 22 and Fig. 7). Had ν been much slower, the polarization would have recovered at least partially. In these circumstances a field of 2 kG which is equivalent to $\omega_L = 170 \text{ MHz}$ should have “decoupled” the relaxation. This is not happening. The solid lines in Fig. 8 represent the expected decoupling which is very different from the observed one. A model has been proposed to explain this problem [42], which received the name sporadic dynamic (SD) [43][44].

In this model, the sample is not relaxing the muon spin all the time but only for a fraction f of the time, as demonstrated in Fig. 16. In zero field it is clear that such a case will lead to sporadic dynamic polarization $\overline{P}_z^{\text{sd}}(\nu, 0, \Delta, t) = \overline{P}_z(\nu, 0, \Delta, ft)$. However, even when the H is applied, the polarization changes only when the internal field relaxes the muon spin. In other words, the flat parts in Fig. 16 stay flat even when H is on. Therefore we expect $P_z^{\text{sd}}(\nu, \omega_L, \Delta, t) = \overline{P}_z(\nu, \omega_L, \Delta, ft)$ for all values of ω_L . Since ν , ω_L , and Δ always enter the relaxation function as a product with t (for example see Eq. 21) we must have $\overline{P}_z^{\text{sd}}(\nu, \omega_L, \Delta, t) = \overline{P}_z(f\nu, f\omega_L, f\Delta, t)$.

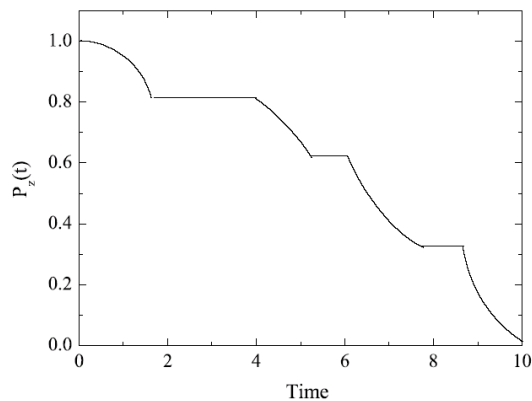


Fig. 16. Muon relaxation function in a case where the muons relax only sporadically at certain intervals of time.

When analyzing the data we are actually estimating $f\Delta$ and $f\nu$ to be 10 MHz and $\overline{P}_z^{\text{sd}} = \overline{P}_z(10, f\omega_L, 10, t)$. Therefore, the effect of the H is reduced by factor f . In the fraction of the time the field is turned on, Δ and ν are

much higher than 10 MHz. This is the reason we do not see decoupling. This model is very successful in explaining μ SR data.

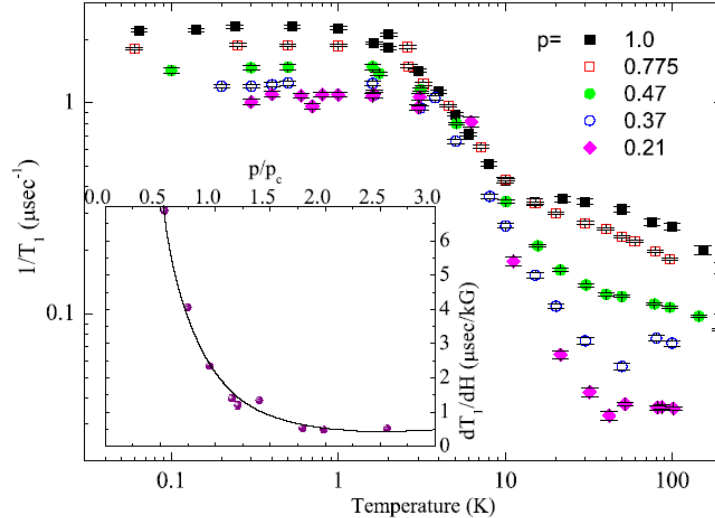


Fig. 17. Temperature dependence of the muon relaxation rate $1/T_1$ at $H=50\text{G}$. Inset, the rate at which T_1 varies with field as a function of magnetic ion concentration p normalized by the percolation threshold p_c .

The model could lead to two interpretations. The first one is that most of the time the field at the muon site is zero due to singlet formation but every now and then a singlet breaks giving rise to a fluctuating field and relaxation [42]. The problem with this interpretation is that the muon relaxation is temperature-independent below 2-3K, similar to the case presented in Fig. 17. This usually happens when the system is in its ground state. But in the ground state there cannot be time evolution, namely, the field cannot turn on and off and the muon spin cannot relax. If the system is not in the ground state at $T \simeq 2\text{ K}$, then a lower energy scale, below about 100 mK, must exist which separates the ground from the first excited states. Accordingly, the constant relaxation observed for $100\text{mK} \leq T \leq 2\text{ K}$, would arise from the quantum fluctuations within a manifold of weakly coupled nearly degenerate states. Another possibility is that the muon is hopping, although not evenly, between two sites with different relaxation rates. This, however, is also unusual at such low temperatures. A full description of the muon spin behavior in SCGO and similar systems is still lacking.

2.6 Persistent dynamics and lattice distortions in the pyrochlore lattice

If there is one common message deducible from the study of frustrated magnets by μ SR it is that these systems maintain a fluctuating part of the moment even when the temperature is lowered much below the coupling energy scale. This is manifested in the saturation of $1/T_1$ upon cooling. In zero field $1/T_1$ is given by Eq. 23. Therefore, for $1/T_1$ to remain finite, at least part of the moment must continue to fluctuate and Δ cannot be zero. While both T_1 and Δ can vary from system to system, the typical scale for ν is μsec^{-1} .

In Fig. 17 we present what might be the canonical example of persisting fluctuations to the lowest temperatures, $\text{Tb}_2\text{Ti}_2\text{O}_7$ [46]. The full black symbols denote $1/T_1$ over a wide temperature range. The increase in $1/T_1$ upon cooling indicates that ν decreases, namely, the spin fluctuations slow down. However, in standard magnets, at some temperature long range order or spin freezing sets in, and the amplitude of the fluctuations δB (see Eq. 19) also decrease upon cooling. This is manifested in a decrease in Δ^2 upon cooling. The net result is a peak in $1/T_1$ at, or close to, the critical temperature. The $1/T_1$ peak is missing in $\text{Tb}_2\text{Ti}_2\text{O}_7$ suggesting that no static magnetic moment develops in this system. Similar results were obtained in other pyrochlore lattices such as $\text{Tb}_2\text{Sn}_2\text{O}_7$ [47] and $\text{Gd}_2\text{Ti}_2\text{O}_7$ [44].

This conclusion leads to yet another open question in this area of research, namely, which type of excitation will dominate at low temperatures: spin wave, spinless, or spinons? This can be examined by measuring $1/T_1$ as a function of magnetic ion concentration p above and below the percolation threshold p_c . A strong dependence of $1/T_1$ on p close to p_c would suggest that the fluctuations emerge from a collective phenomenon. In contrast, if $1/T_1$ varies smoothly across p_c it would suggest that the excitations are local in nature and impartial to the coverage of the lattice. In Fig. 17 $1/T_1$ is presented for $(\text{Tb}_p\text{Y}_{1-p})_2\text{Ti}_2\text{O}_7$ samples in which the Tb magnetic ion is replaced by non-magnetic Y [49]. Clearly the fluctuations have similar behavior both above and below the percolation threshold which is at $p_c = 0.39$ [45].

Moreover, the muon T_1 was found to be a linear function of H [49]. This is a very different behavior from Eq. 22 and suggests that the field correlation does not decay exponentially but rather with a power law. In this case, the dynamic properties of the system could be collected into dT_1/dH . In the inset of Fig. 17 we show dT_1/dH as a function of p . This quantity shows no anomaly at p_c , suggesting that T_1 is controlled by local excitations.

Finally, as in the case of $\text{Li}_2\text{VOSiO}_4$ (see Sec. 2.2), magnetoelastic coupling is a very important interaction [50, 51] in the pyrochlore system as well. It could lead to a lattice deformation in order to relieve the frustration. In fact, regardless of how small this interaction is, it will cause some lattice deformation. In other words, there is no such thing as a perfect Heisenberg pyrochlore lattice since it must distort. Of course, for very small magnetoelastic coupling the distortion could be undetectably small. Nevertheless, the investigation

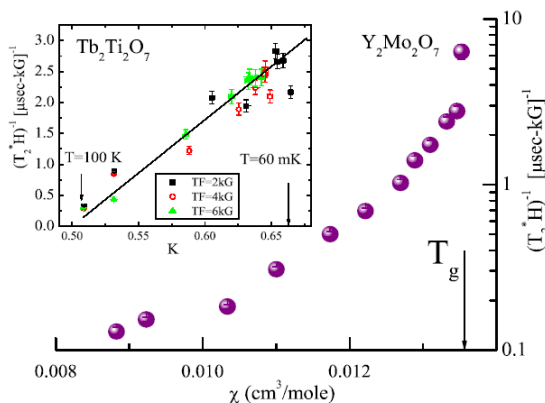


Fig. 18. $1/T_2^*$ normalized by the field for $Y_2Mo_2O_7$ versus susceptibility on a semi-log scale, with the temperature as an implicit parameter. Inset, $1/T_2^*$ normalized by the field for $Tb_2Ti_2O_7$ on a linear scale.

of the ground state in the presence of magnetoelastic coupling is a growing theoretical sub-field accompanied by experimental search for this effect.

As explained above, a comparison between the muon relaxation rate and the muon shift or macroscopic susceptibility can provide a hint about lattice deformations. For example, in the pyrochlore $Y_2Mo_2O_7$, $1/T_2^*$ depends exponentially on the susceptibility. This is demonstrated in Fig. 18 on a semi-log scale. The fact that the lattice parameters in $Y_2Mo_2O_7$ vary upon cooling received confirmation also from NMR [51] and x-ray [52] experiments. In contrast, the lattice of $Tb_2Ti_2O_7$ does not distort [53], and, indeed, $1/T_2^*$ depends linearly on the susceptibility as shown in the inset of Fig. 18.

Acknowledgements

The authors would like to acknowledge Y. Furukawa and K. Kanoda for contributing to this manuscript with the figures reporting their results. A. Keren acknowledges support by the Israel U.S.A. binational science foundation.

References

1. C. P. Slichter in *Principles of Magnetic Resonance* (Springer, Berlin, 1990) 3rd Ed.; A. Abragam in *Principles of Nuclear Magnetism* (Oxford University Press, New York, 1961).

2. Muon science, edited by S. L. Lee, S. H. Kilcoyne and R. Cywinski (IOP Publishing, Bristol and Philadelphia, 1999); A. Schenck, *Muon Spin Rotation: Principles and Applications in Solid State Physics* (Adam Hilger, Bristol, 1985); S. Blundell, *Contemporary Physics* **40**, 175 (1999).
3. C.H. Pennington and C.P. Slichter, *Phys. Rev. Lett.* **66**, 381 (1991).
4. R.Ofer, S. Levy, A. Kanigel, and A. Keren, *Phys. Rev. B* **73**, 012503, (2006).
5. I. R. Mukhamedshin, H. Alloul, G. Collin, and N. Blanchard, *Phys. Rev. Lett.* **93**, 167601 (2004)
6. L. Limot, P. Mendels, G. Collin, C. Mondelli, B. Ouladdiaf, H. Mutka, N. Blanchard, and M. Mekata, *Phys. Rev. B* **65**, 144447 (2002)
7. see for instance H. Alloul, J. Bobroff, M. Gabay, and P. J. Hirschfeld, *Rev. Mod. Phys.* **81**, 45 (2009) and references therein
8. R. S. Hayano, Y. J. Uemura, J. Imazato, N. Nishida, T. Yamazaki, and R. Kubo, *Phys. Rev. B* **20**, 850 (1979).
9. A. Keren, L. P. Le, G. M. Luke, B. J. Sternlied, W. D. Wu, Y. J. Uemura, S. Tajima, S. Uchida, *Phys. Rev. B* **48**, 12926 (1993).
10. W. H. Press, B. P. Flannery, A. A. Teukolsky, and W. T. Vetterling, *Numerical Recipes* (Cambridge University Press, Cambridge, 1989).
11. J. H. Brewer, D.R. Harshman, R. Keitel, S. R. Kreitzman, G. M. Luke, D. R. Noakes, and R. E. Turner, *Hyperfine Interactions* **32**, 677 (1986).
12. Y. J. Uemura T. Yamazaki D. R. Harshman M. Senab, and E. J. Ansaldo, *Phys. Rev. B* **31** (1985).
13. A. Keren, *J. Phys.: Condens. Matter* **16**, 1 (2004).
14. A. Keren, *Phys. Rev. B* **50**, 10039 (1994).
15. D. Gatteschi, A. Caneschi, L. Pardi, and R. Sessoli, *Science* **265**, 54 (1994)
16. Y. Furukawa, Y. Nishisaka, K. Kumagai, P. Kögerler, and F. Borsa, *Phys. Rev. B* **75**, 220402 (2007)
17. D. Prociassi, A. Lascialfari, E. Micotti, M. Bertassi, P. Carretta, Y. Furukawa, and P. Kögerler, *Phys. Rev. B* **73**, 184417 (2006)
18. R. Melzi, P. Carretta, A. Lascialfari, M. Mambrini, M. Troyer, P. Millet and F. Mila, *Phys. Rev. Lett.* **85**, 1318 (2000)
19. R. Melzi, S. Aldrovandi, F. Tedoldi, P. Carretta, P. Millet and F.Mila, *Phys. Rev. B* **64**, 024409 (2001)
20. A. Bombardi, F. de Bergevin, S. Di Matteo, L. Paolasini, P.Carretta, J. Rodriguez-Carvajal, P. Millet and R. Caciuffo, *Phys.Rev. Lett.* **93**, 027202 (2004)
21. P. Carretta, R. Melzi, N. Papinutto and P. Millet, *Phys. Rev. Lett.* **88**, 047601 (2002)
22. P. Carretta, N. Papinutto, R. Melzi, P. Millet, S. Gouthier, P. Mendels and P. Wzietek, *J. Phys.: Condens. Matter* **16**, S849-S856 (2004)
23. P. Carretta, N. Papinutto, C. B. Azzoni, M. C. Mozzati, E. Pavarini, S. Gonthier, and P. Millet, *Phys. Rev. B* **66**, 094420 (2002)
24. N. Papinutto, P. Carretta, S. Gonthier and P. Millet, *Phys. Rev. B* **71**, 174425 (2005)
25. P. Chandra, P. Coleman and A. I. Larkin, *Phys. Rev. Lett.* **64**, **88** (1990)
26. L. K. Alexander, N. Büttgen, R. Nath, A. V. Mahajan and A. Loidl, *Phys. Rev. B* **76**, 064429 (2007); A. Olariu, P. Mendels, F. Bert, B. G. Ueland, P. Schiffer, R. F. Berger, and R. J. Cava, *Phys. Rev. Lett.* **97**, 167203 (2006)

27. Y. Kurosaki, Y. Shimizu, K. Miyagawa, K. Kanoda, and G. Saito, Phys. Rev. Lett. **95**, 177001 (2005); A. Kawamoto, Y. Honma, and K. Kumagai, Phys. Rev. B **70**, 060510 (2004)
28. Y. Shimizu, K. Miyagawa, K. Kanoda, M. Maesato, and G. Saito, Phys. Rev. Lett. **91**, 107001 (2003)
29. P.W. Anderson, Mater. Res. Bull. **8**, 153 (1973)
30. M. L. Foo, Y. Wang, S. Watauchi, H. W. Zandbergen, T. He, R. J. Cava, and N. P. Ong, Phys. Rev. Lett. **92**, 247001 (2004)
31. J. Bobroff, G. Lang, H. Alloul, N. Blanchard, and G. Collin, Phys. Rev. Lett. **96**, 107201 (2006)
32. J. L. Gavilano, B. Pedrini, K. Magishi, J. Hinderer, M. Weller, H. R. Ott, S. M. Kazakov, and J. Karpinski, Phys. Rev. B **74**, 064410 (2006)
33. G. Lang, J. Bobroff, H. Alloul, P. Mendels, N. Blanchard, and G. Collin, Phys. Rev. B **72**, 094404 (2005)
34. C. de Vaulx, M.-H. Julien, C. Berthier, S. Hübert, V. Pralong, and A. Maignan, Phys. Rev. Lett. **98**, 246402 (2007)
35. A. Olariu, P. Mendels, F. Bert, B. G. Ueland, P. Schiffer, R. F. Berger, and R. J. Cava, Phys. Rev. Lett. **97**, 167203 (2006)
36. H. Ikegami, R. Masutomi, K. Obara and H. Ishimoto, Phys. Rev. Lett. **85**, 5146 (2000)
37. M. Roger, C. Bäuerle, Yu. M. Bunkov, A.-S. Chen and H. Godfrin, Phys. Rev. Lett. **80**, 1308 (1998); H. Ishimoto, R. Masutomi, H. Ikegami, Y. Karaki and A. Yamaguchi, J. Phys. Chem. Solids **66**, 1417 (2005).
38. O. Ofer and A. Keren, accepted to PRB.
39. A. Olariu, P. Mendels, F. Bert, F. Duc, J. C. Trombe, M. A. de Vries, and A. Harrison, Phys. Rev. Lett. **100** 087202 (2008).
40. T. Imai, E. A. Nytko, B. M. Bartlett, M. P. Shores and D. G. Nocera, Phys. Rev. Lett. **100** 077203, (2008).
41. O. Ofer, A. Keren, E. A. Nytko, and M. P. Shores, cond-matt/0610540.
42. Y. J. Uemura *et al.*, Phys. Rev. Lett. **73**, 3306 (1994).
43. D. Bono, *et al.* Phys. Rev. Lett. **93**, 187201 (2004).
44. A. Yaouanc, Physica B **374-375**, 145-147 (2006).;
45. C. L. Henley, Can. J. Phys. **79**, 1307 (2001).
46. S. R. Dunsiger *et al.*, Phys. Rev. B **54**, 9019 (1996).
47. P. Dalmas de Réotier, A. Yaouanc, L. Keller, A. Cervellino, B. Roessli, C. Baines, A. Forget, C. Vaju, P. C. M. Gubbens, A. Amato, and P. J. C. King, Phys. Rev. Lett. **96**, 127202 (2006).
48. A. Yaouanc, P. Dalmas de Réotier, V. Glazkov, C. Marin, P. Bonville, J. A. Hodges, P. C. M. Gubbens, S. Sakarya, and C. Baines, Phys. Rev. Lett. **95**, 047203 (2005).
49. A. Keren., S. Gardner, G. Ehlers, A. Fukaya, E. Segal, and Y. J. Uemura, Phys. Rev. Lett. **92**, 107204 (2004).
50. K. Terao, J. Phys. Soc. Japan **65**, 1413 (1996); Y. Yamashita and K. Ueda, Phys. Rev. Lett. **85**, 4960 (2000); S.-H. Lee, C. Broholm, T. H. Kim, W. Ratcliff II, and S-W. Cheong, Phys. Rev. Lett. **84**, 3718 (2000); O. Tchernyshyov, R. Moessner, and S. L. Sondhi, Phys. Rev. Lett. **88**, 067203 (2002); J. Richter, O. Derzhko, and J. Schulenburg, Phys. Rev. Lett. **93**, 107206 (2004); D. L. Bergman, R. Shindou, G. A. Fiete, and L. Balents, Phys. Rev. B **74**, 134409 (2006), K. Penc, N. Shannon, and Hiroyuki Shiba, Phys. Rev. Lett. **93**, 197203 (2004) ; F. Wang and A. Vishwanath, cond-mat/0709.3546.

51. A. Keren and J. S. Gardner, Phys. Rev. Lett. **87**, 177201 (2001).
52. O. Ofer *et al.* in preparation.
53. S.-W. Han, J. S. Gardner, and C. H. Booth, Phys. Rev. B **69**, 024416 (2004).